AD_____

Award Number: DAMD17-99-1-9316

TITLE: Monochromatic Mammographic Imaging Using X-ray Polycapillary Optics

PRINCIPAL INVESTIGATOR: Francisca Sugiro
Carolyn McDonald, Ph.D.

CONTRACTING ORGANIZATION: The Research Foundation of SUNY
University of Albany
Albany, New York 12222

REPORT DATE: June 2001

TYPE OF REPORT: Annual Summary

PREPARED FOR: U.S. Army Medical Research and Materiel Command
Fort Detrick, Maryland 21702-5012

REPORT DOCUMENTATION PAGE

Form Approved
OMB No. 074-0188

1. AGENCY USE ONLY (Leave blank)	2. REPORT DATE	3. REPORT TYPE AND DATES COVERED
	June 2001	Annual Summary (1 Jun 00 - 31 May 01)

4. TITLE AND SUBTITLE
Monochromatic Mammographic Imaging Using X-ray Polycapillary Optics

5. FUNDING NUMBERS
DAMD17-99-1-9316

6. AUTHOR(S)
Francisca Sugiro
Carolyn McDonald, Ph.D.

7. PERFORMING ORGANIZATION NAME(S) AND ADDRESS(ES)
The Research Foundation of SUNY University of Albany
Albany, New York 12222

E-Mail: fs5699@csc.albany.edu

8. PERFORMING ORGANIZATION REPORT NUMBER

9. SPONSORING / MONITORING AGENCY NAME(S) AND ADDRESS(ES)
U.S. Army Medical Research and Materiel Command
Fort Detrick, Maryland 21702-5012

10. SPONSORING / MONITORING AGENCY REPORT NUMBER

11. SUPPLEMENTARY NOTES

12a. DISTRIBUTION / AVAILABILITY STATEMENT
Approved for Public Release; Distribution Unlimited

12b. DISTRIBUTION CODE

13. ABSTRACT ***(Maximum 200 Words)***

Monochromatic parallel beam imaging can produce greater contrast, higher resolution and lower patient absorbed dose. Currently, monochromatic imaging has been restricted to specialized research sources such as synchrotrons. Collimating polycapillary x-ray optics can efficiently collimate the beam from a practical conventional laboratory x-ray source, which will allow monochromatic imaging in a clinical setting.

To verify the optics capability, a molybdenum x-ray point source was used to characterize the collimating polycapillary optic. The transmission is about 39 % at 17.5 keV. The measurements agree quite well with simulations.

Monochromatic imaging was performed using this optic with two different sources, a rotating anode copper source and a low power molybdenum source. The copper source was used for verifying the contrast and resolution off three crystals with different bandwidths: silicon, mica and graphite. The contrast enhancement was 5-6 at 8 keV for both step phantoms and for phantoms containing multiple types of plastic. The angular resolution was measured with the silicon crystal and was found to be more than adequate. The molybdenum x-ray source was also used to measure the contrast. The contrast enhancement was 2 at 17.5 keV for a 45-mm thick phantom containing the usual multiple holes of different depths.

14. SUBJECT TERMS	15. NUMBER OF PAGES
Breast Cancer	36
	16. PRICE CODE

17. SECURITY CLASSIFICATION OF REPORT	18. SECURITY CLASSIFICATION OF THIS PAGE	19. SECURITY CLASSIFICATION OF ABSTRACT	20. LIMITATION OF ABSTRACT
Unclassified	Unclassified	Unclassified	Unlimited

Table of Contents

Introduction:

The American Cancer Society estimated about 43,900 deaths and 178,700 new cases of invasive breast cancer among women in the United States in 1998.[1] Although molecular detection and intervention may provide a more effective treatment modality, currently, screening mammography is the single most effective, low-cost technique for detecting small lesions. Unfortunately, mammographic images have been hampered by the somewhat wide spectrum of radiation emitted by x-ray tubes. This creates fog on the film and increases the dose to the patient. The solution to this problem is imaging with x rays only at the desired energy for the imaging task at hand, so that the images can greatly be improved. Monochromatic imaging is generally only available with synchrotron sources or free electron lasers because of the high intensity needed. Conventional laboratory sources can be monochromatized by using single crystal diffraction, but do not give the desired intensity. Combining polycapillary x-ray optics with conventional x-ray laboratory sources can greatly improve the diffracted beam intensity. Monochromatizing a conventional x-ray source will allow routine screening mammography to take advantage of high contrast, good resolution and reduced patient dose. This technique has enormous potential to become a highly effective tool for imaging carcinomas in a low-cost clinical environment.

Body:
Principle:

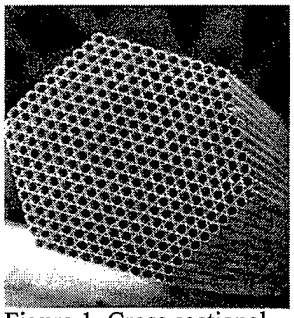

Figure 1. Cross sectional electron picture of polycapillary fiber 500 μm in diameter. This fiber has approximately 100 channels, each 50 μm in diameter.

Monochromatic imaging involves a collimating optic which makes the x-ray radiation parallel, and a diffracting crystal, which makes the beam monochromatic (a single energy wavelength).

The collimating optic is a polycapillary x-ray optic. Polycapillary fibers are bundles of hollow glass capillary tubes with inner diameter as small as a few microns. X rays striking the interior of the glass tubes at grazing incidence can be guided down the tube by total external reflection. The capillaries guide x rays in similar manner as fiber optics guide light. A cross-section of a polycapillary bundle is shown in figure 1. Thousands of these bundles are laced through an aligned metal grids to form a large area (10 mm by 10 mm) multi-fiber collimating polycapillary optic.

Optic Characterizations:

The measurements of the prototype optic are almost completed. The optic was characterized with a small molybdenum point source and germanium detector. The experimental set-up is shown in figure 2. The parameters of the optic are shown in table 1.

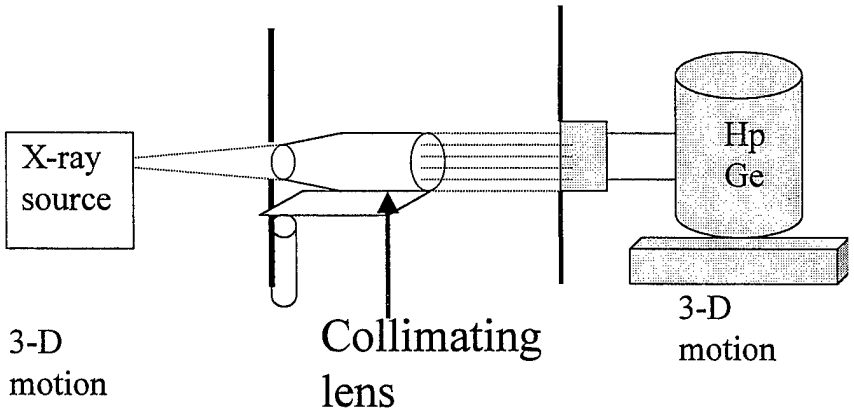

Figure 2. Experimental set-up for characterization.

Collimating optic parameters	
Length	127 mm
Input	8.07 X 8.07 mm
Output	10 X 10 mm
Focal distance	250 mm
Acceptance angle	1.8°
Fiber Outer diameter	510 μm
Channel diameter	10 μm

Table 1. A076-H9 parameters

Transmission as a function of energy

The measured transmission as a function of x-ray energy is shown in figure 3. Since the simulation programs are for single fibers, we integrated the single fiber simulation results to model into an optic for this comparison. Our CXO simulation includes waviness and roughness. Waviness is random tilt of the glass surface. The tilt angles are assumed to have a Gaussian distribution of width w. Surface roughness has a short wavelength, generally on the order of few microns or less, and causes photon transmission into the glass of a fiber, as well as diffuse scattering. This can be accounted for with an equation based on the roughness height and correlation length. The simulations results decreases with the addition of these factors from the highest curve to the second lowest in figure 3. A waviness value of 0.15 mrad and roughness of 0.5 nm were used as typical for this type of glass. However, the results still overestimate the transmission at the highest energy. Since it is known that the optic shape is not circular, the effect of the optic shape was investigated. We decided to model its shape using cubic polynomial. Since CXO's simulation program does not have cubic bending, only circular bending, we used another code, which has cubic bending but no waviness and roughness. This other code is proprietary from the manufacturer, X-ray Optical Systems, Inc. As expected the ideal cubic simulation overestimates the transmission. To include the effects of waviness and

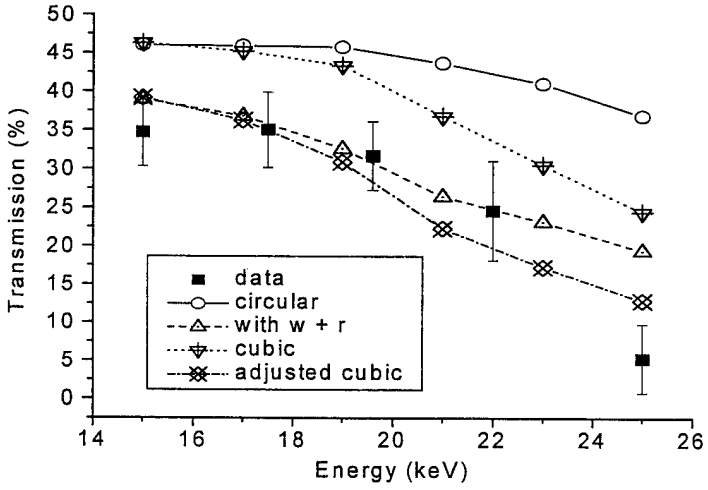

Figure 3. Transmission versus energy with their simulations. 'w' and 'r' refer to waviness and roughness, respectively.

roughness, the percentage difference between the ideal circular and the circular with waviness and roughness was percentage subtracted from ideal cubic simulation. This gives finally the adjusted cubic shown in figure 3.

Transmission as a function of x-ray entrance angle

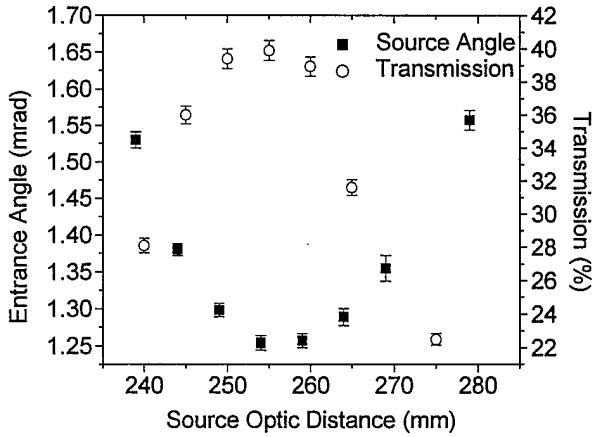

Figure 4. Transmission and source angle as a function of source optic distance.

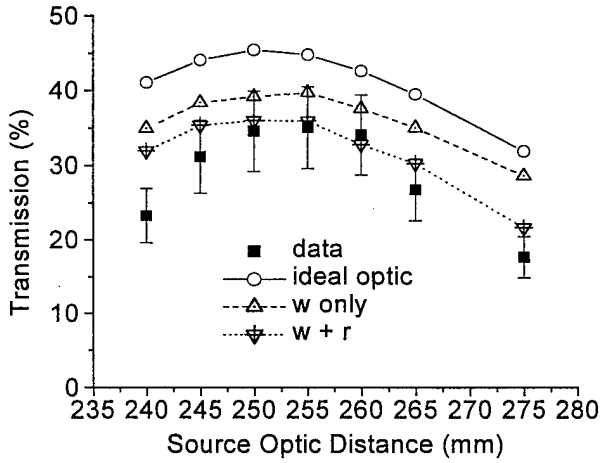

Figure 5. Transmission versus source optic distance.

Energy (keV)	STD/Mean (%)
15	21.7
17.5	24.8
19.6	31.0
22	34.3
25	38.6

Table 2. Uniformity of output of the optic at each energy window.

To find the best aligned position for the optic, source scans were performed. The scans were taken with the source very close to the source, very far and in between. The widths of all the scans are divided by the source-optic distances to give the x-ray source acceptance angles. This is plotted in figure 4. The distance with the minimum acceptance angle and the highest transmission is the focal distance. The depth of field, the distance over which the transmission and entrance angle do not vary by more than 10 %, is about 10 mm. The transmission was measured with an energy window of 2 keV centered at 17.5 keV Kα of molybdenum.

The experimental values of transmission versus source optic distance are compared to three simulations: the ideal optic, single fiber with waviness, and single fiber with waviness and roughness as shown in figure 5.

Transmission uniformity

The uniformity was measured with a 2.1-mm diameter pinhole scanned across the output of the optic for 15 seconds at each step. The distance between each step was 14 mm/17 steps = 0.824 mm. The uniformity for each energy window is shown in

table 2. Figure 6 shows the output of the optic taken with a Fuji imaging plate.

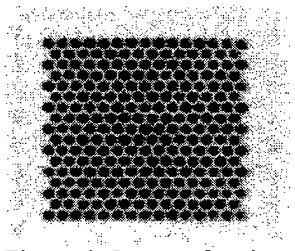

Figure 6. Output of optic taken with Fuji imaging plate.

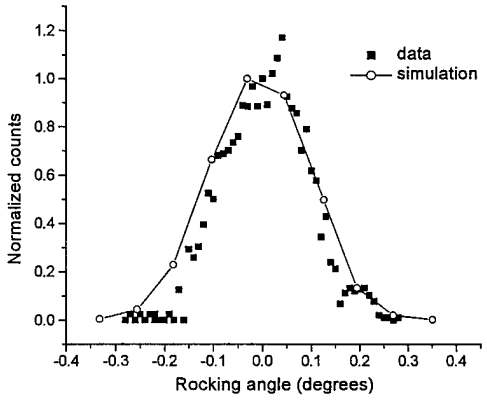

Figure 7. Exit angle divergence of the optic with its simulation including waviness and roughness.

Output divergence

Since the width of the silicon (100) diffraction rocking curve is much smaller than the measured divergence of the x rays, the contribution of the width of the silicon (100) rocking curve can be neglected. The measured angular profile of the diffracted x-ray intensity is entirely due to the optic divergence and is shown in figure 7. The width is 4.0 ± 0.5 mrad. The crystal was tuned to the Kβ rather than the Kα peak because the Kα doublet cannot be resolved, and so the contributes extra broadening. The simulation, which included both waviness and roughness of the glass surface, has a width of 4.3 mrad.

Output divergence uniformity

Output divergence uniformity measurements will be performed when the source, which is currently being repaired, returns.

Monochromatic Imaging:

The experimental set-up for this section is shown in figure 8.

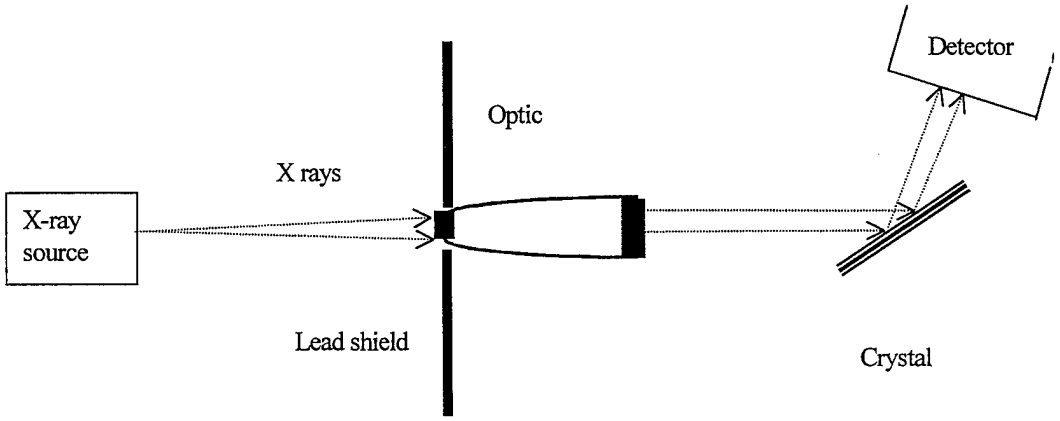

Figure 8. Experimental set-up for monochromatic imaging.

Total Photon Flux

The photon flux calculation is currently in progress.

Beam Uniformity

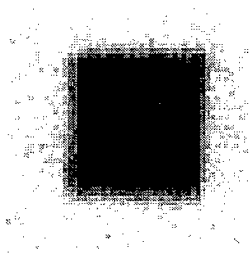

Figure 9. Beam uniformity at 8 keV taken with a Fuji image plate.

The uniformity of the beam at 8 keV is 27.5 %. The large deviations are due to the fiber structure.

Resolution

A knife-edge made of tantalum was placed after the monochromatic parallel beam. An image plate was placed 300 mm from the knife-edge to overcome the 50-μm resolution. Tantalum was chosen so to reduce the x-ray fluorescence background. The intensity profile was measured. The derivative of the intensity profile was calculated. The result consists of the overlapping doublet of $K\alpha_1$ and $K\alpha_2$. The Gaussian width of the $K\alpha_1$ line is given in table 3 for silicon and mica and for the $K\alpha$ unresolved total peak for graphite. The intensity profiles measured with silicon, mica, and graphite crystals are shown in figure 10. The theoretical calculation, of angular resolution takes into account the energy width of the characteristic lines, the optic divergence, and the angular bandwidth of the crystal.[2]

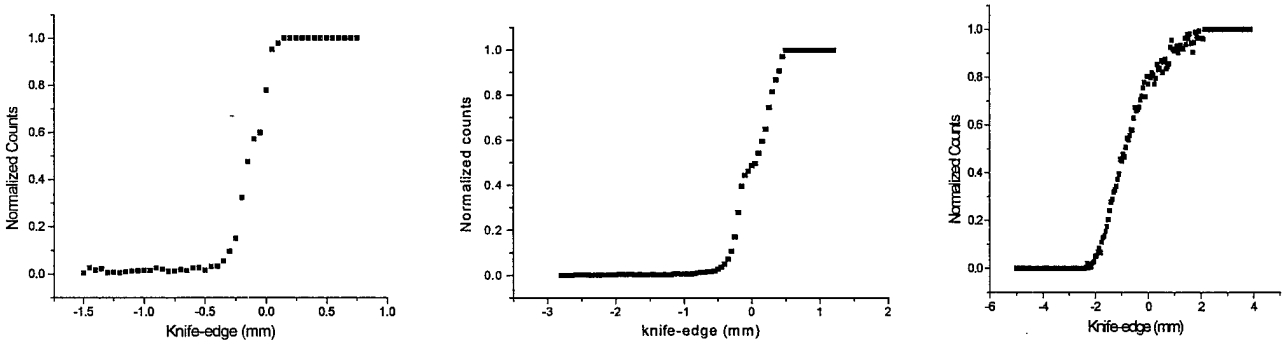

Figure 10. Resolution profiles obtained with silicon (a), mica (b) and graphite (c) crystals incident angles.

Crystals:	Manufacturer's specification for α (mrad):	Measured rocking curve width (mrad):	Angular width of knife-edge image (mrad):	σ, Theory (mrad), with detector with 50 μm pixels	σ, Theory (mrad), with an ideal detector	Resultant resolution for 50-mm thick patient for an ideal detector (lp/mm)
Silicon	0.02	4.0 ± 0.1	0.54 ± 0.02	0.47	0.43	23
Mica	0.4	4.4 ± 0.2	0.78 ± 0.04	0.52	0.48	20
Graphite	35 – 87	42.5 ± 1.1	6.5 ± 0.5	4.5	4.5	2

Table 3. Rocking curves and resolution measurements using three different crystals. The rocking curve widths are due to the combined effects of the angular bandwidth of the crystal and the 4-mrad output divergence of the optic. The energy width for graphite is taken to include the whole Kα doublet.

Scatter fraction

Since the optic is only 10 mm by 10 mm, the measured scatter fraction is essentially zero, particularly for the 8 keV case, where the phantom is also quite thin.

Contrast Enhancement

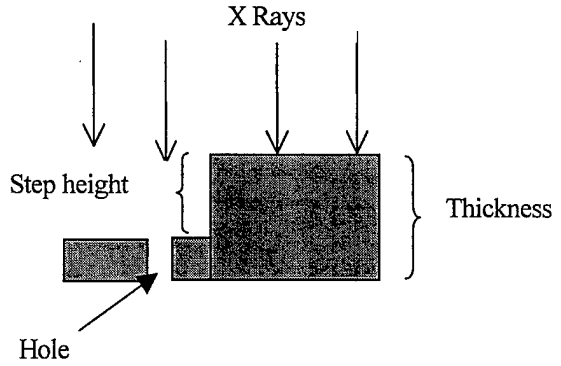

Figure 11. Shape of the polypropylene step phantom used for figure 12 and table 4.

Polypropylene step phantoms of different heights were tested in the polychromatic and monochromatic cases. For the latter case, the phantom was placed after the crystal and before the detector. In the polychromatic case images were taken with the phantom placed without the optic and crystal. The images are taken with a 50-micron resolution imaging plate. The construction of these phantoms with different step heights is shown in figure 11.

The contrast arising from the two thicknesses are compared in both the conventional and the monochromatic cases in table 2. The images for five different step heights are shown in figure 12. In the polychromatic case, the theoretical intensities are averaged from 7

keV to 19 keV. The tube voltage was 20 kVp. The data from all three crystals agree with each other and the theoretical calculation. The contrast enhancement is greater than 5 for monochromatic imaging at 8 keV.

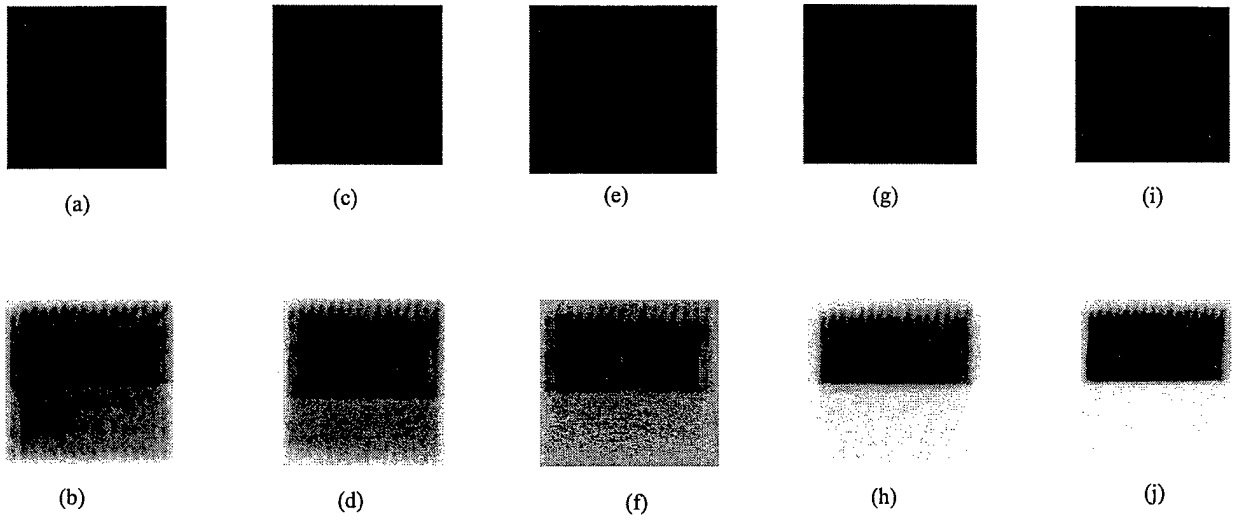

Figure 12. Image plate data from five different polypropylene step phantoms. The top row is measured without optic (conventional), the bottom row is measured in the monochromatic case. Column (a-b) is the phantom with a step height of 1.5 mm, column (c-d) with 2.0 mm, column (e-f) with 6.6 mm, column (g-f) with 10.6 mm, and column (i- j) with 15.5 mm. Notice contrast is already visible in the monochromatic case for a even for the lowest step height.

In addition to the step phantoms, monochromatic images were also measured for a phantom consisting of two compositions of plastic, polypropylene (PP) and polyvinyl chloride (PVC) with the approximately the same thickness (0.5 mm). The density and absorption constants were taken from NIST[3] as 0.9 g/cm^3 and 3.30 for PP and 1.4 g/cm^3 87.86 for PVC, respectively. Table 3 summarizes the experimental and the theoretical values for both the polychromatic and monochromatic cases.

Step-height (mm):	Polychromatic Contrast:	
	Data: (without optic)	Theory:
1.5	0.2 ± 0.1	0.2
2.0	0.2 ± 0.1	0.2
6.6	0.4 ± 0.1	0.4
10.6	0.8 ± 0.1	0.8
15.5	1.2 ± 0.1	1.2

Step-height (mm):	Monochromatic Contrast:			
	Data:			Theory:
	Silicon:	Mica:	Graphite:	
1.5	0.6 ± 0.4	0.7 ± 0.1	0.7 ± 0.3	0.6
2.0	0.7 ± 0.3	0.9 ± 0.2	1.0 ± 0.2	0.7
6.6	2.2 ± 0.5	1.8 ± 0.3	2.1 ± 0.2	2.2
10.6	4.3 ± 0.5	3.8 ± 0.2	4.2 ± 0.3	3.8
15.5	5.3 ± 0.4	5.2 ± 0.2	5.1 ± 0.5	5.2

Step-height (mm):	Data Contrast Ratio:			Theory Contrast Ratio:
	Silicon:	Mica:	Graphite:	
1.5	3.0 ± 2.6	3.3 ± 1.3	3.6 ± 2.6	3.0
2.0	4.1 ± 2.5	5.4 ± 2.2	5.8 ± 2.6	3.5
6.6	5.4 ± 2.5	4.6 ± 1.8	5.4 ± 1.9	5.7
10.6	5.3 ± 1.1	4.6 ± 0.7	5.2 ± 0.8	4.8
15.5	4.4 ± 0.6	4.3 ± 0.5	4.2 ± 0.7	4.3

Table 4. Comparison for step phantoms of contrast with silicon, mica, and graphite crystals to the polychromatic contrast for conventional imaging.

Cases:		Contrast:		Contrast Ratio:	
		Data	Theory	Data	Theory
Polychromatic:		0.5 ± 0.1	0.5		
Monochromatic:	silicon	3.0 ± 0.3	2.9	6.4 ± 2.2	6.0
	mica	3.0 ± 0.4		6.4 ± 2.5	
	graphite	2.6 ± 0.2		5.5 ± 1.9	

Table 5. Contrast of different compositions in both the poly- and monochromatic cases.

An ultra-bright molybdenum Oxford source with tube voltage of 25kVp and low power (10-20 W) was used to measure 45-mm Lucite phantoms with different hole depths.

Each depth was compared without optic and with a combination of optic and crystal at molybdenum Kα line. The theoretical contrast was averaged over 8 to 25 keV. A contrast enhancement of more than a factor of 2 is found experimentally, which agrees with the theoretical calculations. Table 6 summarizes the results.

Depth (mm)	Polychromatic Contrast		Monochromatic Contrast	
	Data	Theory	Data	Theory
35	1.3 ± 0.1	1.3	2.4 ± 0.3	2.9
30	1.2 ± 0.1	1.0	2.1 ± 0.3	2.5
20	0.8 ± 0.1	0.6	1.4 ± 0.4	1.7
15	0.4 ± 0.1	0.5	0.7 ± 0.4	0.8

Depth (mm)	Contrast Enhancement Ratio:	
	Data	Theory
35	1.8 ± 0.6	2.2
30	1.8 ± 0.4	2.5
20	2.2 ± 0.9	2.8
15	1.5 ± 0.9	1.6

Table 6. Contrast at 17.5 keV with 45-mm Lucite phantom.

Key research accomplishments:

• Transmission of the optic is about 39 % at 17.5 keV, which agrees with simulation of integrated ideal fibers. The simulation includes waviness of 0.15 mrad and roughness of height of 0.5 nm and 6 μm correlation length.

• Transmission as a function of entrance angle confirms the focal distance at 250 mm and agrees well with the simulation.

• Divergence is 4.0 mrad ± 0.5 at 8 keV, which agrees with simulation.

• Contrast enhancement of different step height phantoms was enhanced by a factor of 5-6 at 8 keV relative to the conventional polychromatic case.

• Contrast enhancement for a phantom of varying composition was a factor of 6 at 8 keV. These all were in good agreement with the theory.

• At the molybdenum Kα line, 17.5 keV, a contrast enhancement of 2 was measured with a 45-mm thick Lucite phantom, in good agreement with theory.

• The contrast is the same with three crystals, silicon, mica, and graphite, with different bandwidth.

• Contrast is also unchanged for images without collimating optic and after optic.

• The measured angular resolution with a silicon crystal is 0.5 mrad at 8 keV. For a 50-mm thick patient, this angle corresponds to 23 lp/mm

Reportable outcomes

PUBLICATIONS:

1. Sugiro, Francisca R., S. D. Padiyar, C. A. MacDonald, "Characterization of Pre- and Post-Patient Polycapillary X-ray Optics for Mammographic Imaging," **Advances in Laboratory-Based X-ray Sources and Optics**, SPIE vol. 4144, 2000.

2. Sugiro, Francisca R. "Monochromatic Imaging with a Conventional Source Using Polycapillary X-ray Optics," **Physics of Medical Imaging**, SPIE vol. 4320, 2001.

3. C. A. MacDonald, W. M. Gibson, Cari, F. R. Sugiro, Suparmi, "High-contrast radiography with polycapillary x-ray optics," **Advances in Laboratory-Based X-ray Sources and Optics II**, accepted SPIE vol. 4502, 2001.

4. C. A. MacDonald, W. M. Gibson, and F. R. Sugiro "High contrast Imaging with Polycapillary Optics," in **Advances in X-ray Analysis**, accepted Proceedings of the 50th Denver X-ray Conference, 2001.

Abstract

1. Sugiro, Francisca R. and C. A. MacDonald, "Characterization of X-ray Polycapillary Collimating Optics for Monochromatic Imaging," presented in **World Congress on Medical Physics and Biomedical Engineering**, Chicago, IL, July 2000, **Medical Physics** vol 27(6).

CONFERENCE PRESENTATION:

Posters:

1. Sugiro, Francisca R. and C. A. MacDonald, "Characterization of Collimating Polycapillary X-ray Optics for Monochromatic Mammography," **The Department of Defense Breast Cancer Research Program Meeting Era of Hope**, Atlanta, GA, June 2000.

2. C. A. MacDonald, W. M. Gibson, and F. R. Sugiro "High contrast Imaging with Polycapillary Optics," in **Advances in X-ray Analysis**, 50th Denver X-ray Conference, 2001.

Talks:

1. Sugiro, Francisca R. and C. A. MacDonald, "Characterization of X-ray Polycapillary Collimating Optics for Monochromatic Imaging," **World Congress on Medical Physics and Biomedical Engineering**, Chicago, IL, July 2000.

2. Sugiro, Francisca R., S. D. Padiyar, C. A. MacDonald, "Characterization of Pre-and Post-Patient Polycapillary X-ray Optics for Mammographic Imaging," **SPIE's 45th Annual Meeting, the International Symposium on Optical Science and Technology**, San Diego, CA, August 2000.

3. Sugiro, Francisca R. and C. A. MacDonald, "Monochromatic Imaging with Conventional Source Using Polycapillary X-ray Optics," **SPIE's International Symposium on Medical Imaging**, San Diego, CA, Feb 2001.

Conclusions:

The optic characterizations have almost been completed. The simulations show good agreement with the experimental data. There is some non-uniformity due to the fiber structure, which could be reduced by using monolithic optics to decrease the inter-fiber space.

Monochromatic imaging has been performed with a copper rotating anode source, because it was the only intense source we had when this project started. It has been clearly shown that the contrast is significantly better in the monochromatic case than the polychromatic case. The resolution is better than 20 lp/mm in the monochromatic case in comparison with polychromatic case. Towards the end of the second year of the project, we obtained a low power molybdenum source and have made contrast measurements, which show a factor of two enhancement, in agreement with theory.

References:

[1] Christoyianni, Ioanna, et al. "Fast Detection of Masses in Computer-Aided Mammography." **IEEE Signal Processing Magazine** 17.1 (2000): 54-64.

[2] Sugiro, Francisca R. and C.A. MacDonald, "Monochromatic Imaging with a Conventional Source Using Polycapillary X-ray Optics," **Physics of Medical Imaging**, SPIE vol. 4320, 2001.

[3] http://physics.nist.gov/PhysRefData/XrayMassCoef/cover.html

Characterization of Pre- and Post- Patient X-Ray Polycapillary Optics for Mammographic Imaging

Francisca R. Sugiro, Sushil D. Padiyar, C. A. MacDonald*

Center for X-ray Optics, Physics Dept., University at Albany, SUNY, Albany, NY 12222

ABSTRACT

Polycapillary x-ray optics can be used as pre- or post-patient optics to design mammographic imaging systems with higher resolution, greater contrast, and a lower absorbed patient dose. A multi-fiber collimating prototype optic, used as pre-patient beam shaper, provides 39 % transmission efficiency at 17.5 keV, good uniformity, and only 3.9 mrad divergence. Experimental optics characterization results are compared with detailed computer simulations including analysis of optical defects such as channel waviness and bending. The collimating optic was used to produce monochromatic radiation by diffracting from a silicon crystal. The monochromatic contrast, measured at 8 keV with a polypropylene phantom, was 5 times greater than the measured polychromatic contrast.

In addition, post-patient optics, monolithic linearly tapered optics used for "scatter-rejection," were characterized. Measurements included a detailed analysis of optic defects which had been causing poor transmission, only 5 % at 20 keV due to localized glass inclusions. Manufacturing improvements resulted in repeatable transmissions near 50%. These optics result in improved contrast because of scatter transmission of less than 1%.

Pre- and/or post-patient polycapillary x-ray optics technology could greatly improve imaging in mammography.

Keywords: polycapillary x-ray optic, monochromatic, contrast, mammography

1. INTRODUCTION

Polycapillary x-ray optics have been studied for more than a decade.[1] These hollow capillary tubes can control and guide x-ray beams in a similar fashion to the way fiber optics guide light. The channel size of each capillary is 2-50 μm. They are fused into a hexagonal polycapillary fiber of 0.51mm diameter flat to flat. An SEM micrograph of a fiber cross-section is shown in figure 1. These fibers are laced through a metal grid to form multi-fiber collimating optics as shown in figure 2.

Figure 1. Cross-sectional SEM picture of polycapillary fiber 0.51 mm in diameter. This fiber has approximately 100 channels, each 50 μm in diameter.

Collimating optics produce a parallel beam at the output end. At the input end each fiber points towards the source. These optics collect over a wide solid angle from an isotropically emitting conventional laboratory point x-ray source to produce a high flux quasi-parallel beam with low divergence. Collimating optics are attractive to use as a pre-patient optic because they can efficiently collect enough intensity into a low angular bandwidth to use with a monochromator crystal. In the past, monoenergetic beams with sufficient intensity could only be produced with expensive sources such as synchrotrons. With multi-fiber collimating optics, monochromatic beams can be produced with conventional laboratory sources for mammographic imaging.

Linearly tapered monolithic optics are attractive as post-patient optics because they have the potential to reduce scatter transmission more than a conventional mammography grid. Geometric blur is also not increased with magnification as the individual capillary tubes are tapered. This allows mating with a low resolution direct digital detector for data processing. Post-patient optics were studied to assess their potential for a mammography unit. A detailed study of optics defects was performed and resulted in manufacturing improvements.

* Email: c.macdonald@albany.edu

2. MULTI-FIBER COLLIMATING OPTIC CHARACTERIZATION

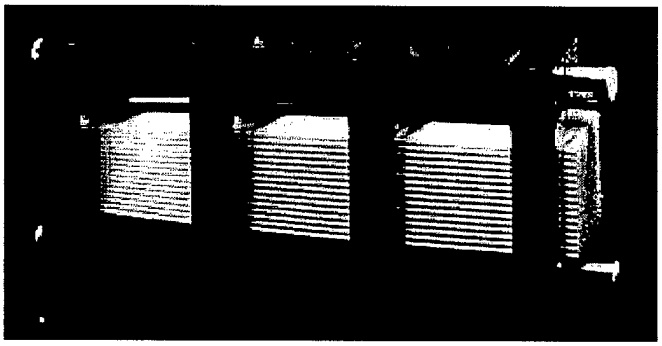

Figure 2. Multi-fiber collimating lens. Output is 20x20 mm, length is 127 mm.

The parameters of this optic are summarized in table 1.

Optic Parameters	Multi-fiber Collimating Optic
Input area	8.07 mm X 8.07 mm
Output area	10 mm X 10 mm
Fiber outer diameter	510 μm
Channel size	10 μm
Focal distance	250 mm
Acceptance angle	1.8 °
Transmission	39 % at 17.5 keV

Table 1. Collimating optic parameters.

2.1. Transmission

Transmission is defined as the ratio of the number of photons collected at the output of the optic over the number of photons at the input. Transmission depends upon the fiber open area and efficient reflections through the fibers. The fiber open area is the part of the fiber which is not blocked by glass walls. The fiber open area of this prototype has been determined to be 64.5%.

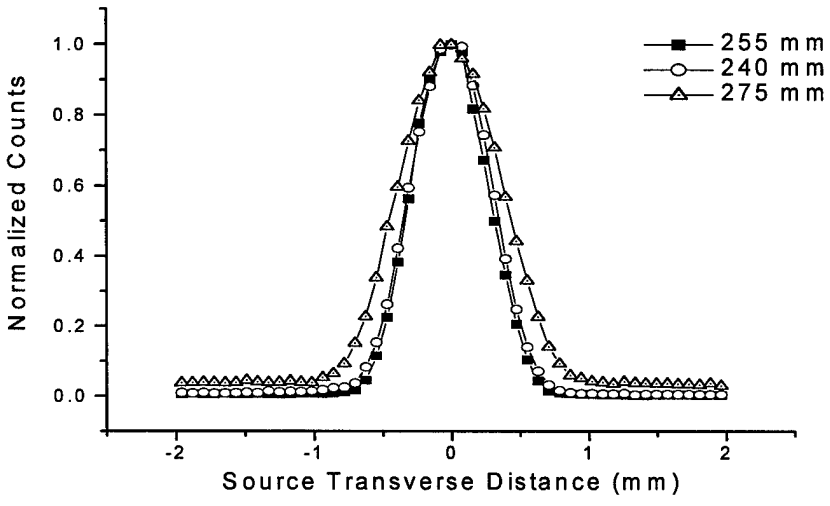

Figure 3. Source scans of the collimating optic distances using a molybdenum source and a germanium detector. The narrowest FWHM, 0.630 ± 0.005 mm, occurs at 255 mm.

The optic was measured with a molybdenum source and Ge solid state detector and also with a copper rotating anode source and NaI detector. The characterization of the optic was performed with the molybdenum point source, which is more easily fitted with simulations and is more appropriate for mammography. However, monochromatic imaging requires higher intensity

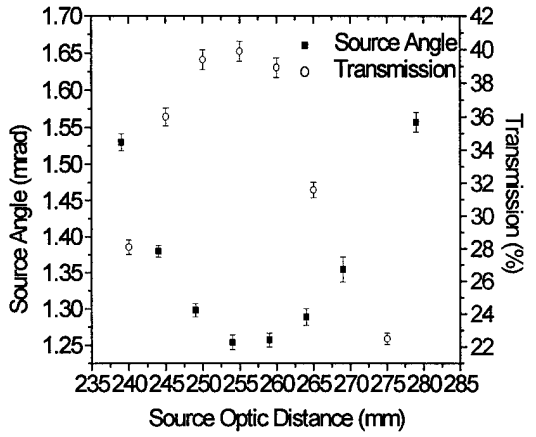

Figure 4. Transmission and source angle as a function of source optic distance for the collimating optic using molybdenum source and germanium detector.

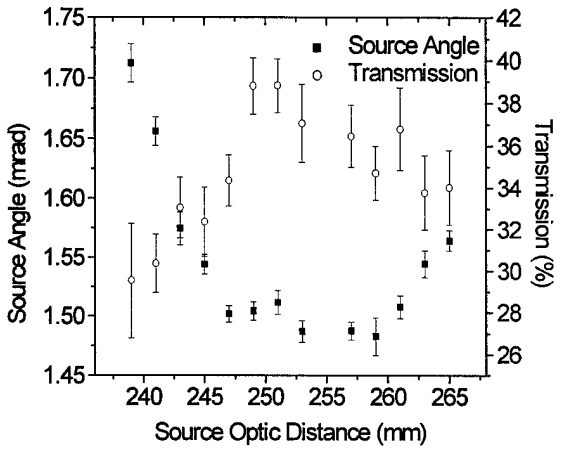

Figure 5. Transmission and source angle as a function of source optic distance using the rotating anode and the NaI detector.

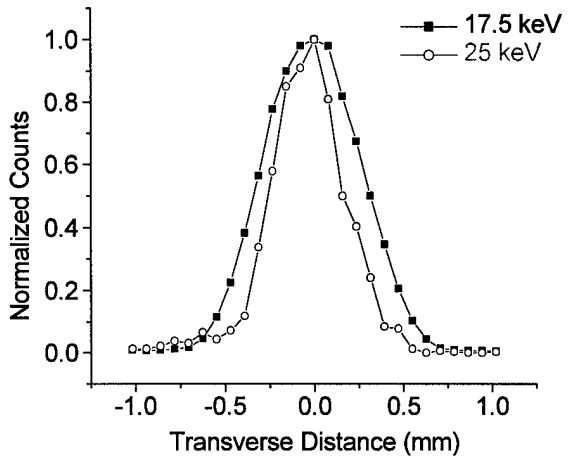

Figure 6. Source scans at different energies using molybdenum source and germanium detector. FWHM at 17.5 keV is 0.63 ± 0.01 mm and at 25 keV is 0.44 ± 0.01 mm

sources, such as the available copper rotating anode. The rotating anode is a line source viewed at 6°. A compact NaI detector was employed because of the feasibility to set it up on actuators and stages.

With the point source at the focal distance of the optic all the x rays from the source hit the fibers at less than the critical angle. The critical angle for total reflection is $\theta_c = E_p/E$. The plasma energy E_p, of borosilicate glass is 32 eV. For an energy of 8 keV, θ_c is 4.0 mrad, and at 20 keV, θ_c is 1.6 mrad.

Scans of transmission as a function of transverse source offset, as the optic is moved off axis, are shown in figure 3. These source scans were taken in the focal plane, a plane closer to the source, and a plane farther from the source. The germanium detector has an energy window of 2 keV centered at 17.5 keV.

The source angle, which is the ratio of the width of the scan curve over the source optic distance, is a minimum at the focal distance. Figure 4 shows source angle and the transmission as a function of the source optic distance taken with the molybdenum source and germanium detector. They show the scatter rejection property of polycapillary optics, because the scans fall sharply as one moves the source transversely. Figure 5 shows these results taken with the rotating anode copper source with the NaI detector. The highest transmission is 39 % for both of these plots and they both occur around 250 mm. The germanium detector window was 2 keV wide centered at the Mo Kα line at 17.5 keV, while the NaI detector had an energy window of 6.5 keV-19.5 keV. The minimum source angle is 1.25 mrad for the molybdenum source and 1.42 mrad for the rotating anode. This difference is due to the line geometry of the rotating anode source. This optic also shows a depth of field of 10 mm. The depth of field is the spatial range over which the transmission remains higher than 90 % of the maximum value as the source is moved along the optical axis.

Source scans were also collected at different energies shown in figure 6. The width of the source scans is narrower at a higher energy, because the critical angle is smaller.

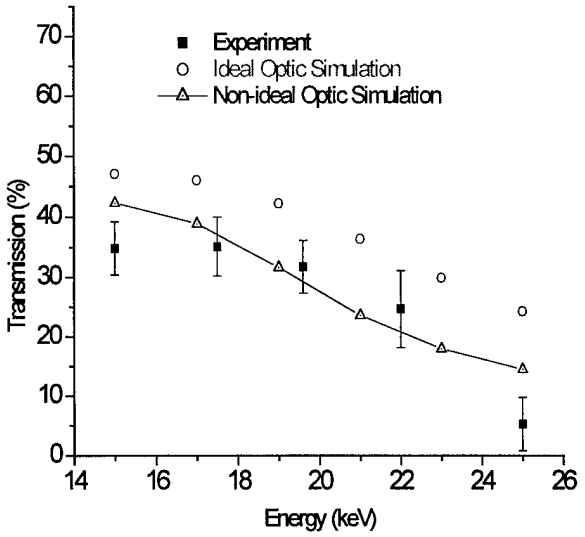

Figure 7. Comparison of experimental and simulation transmissions as a function of energy.

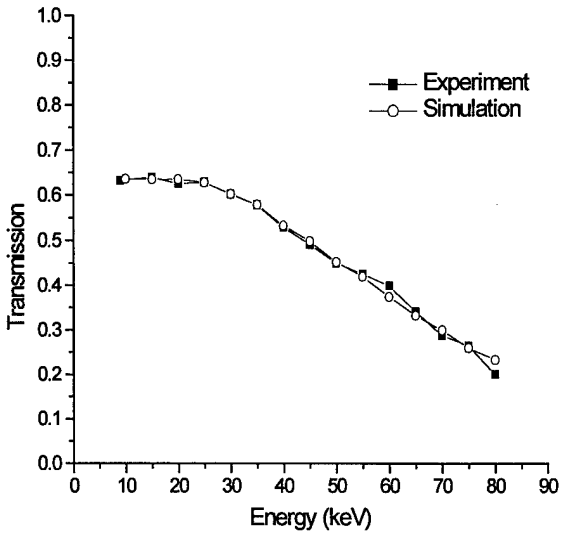

Figure 8. Experiment and simulation as a function of energy for a single fiber from the collimating optic. Simulation is fit with a bending radius of 125 m and waviness 0.15 mrad.

Transmission was also collected as a function of energy, as shown in figure 7. This plot has been fitted with an ideal collimating optic simulation with a fiber open area and the optic fractional open area of 64.5% and 77.5%, respectively.[2] Since this simulation does not include effects due to waviness of the glass, single fiber simulation programs were used to assess these effects.[3] Single fibers used to construct the optic were measured from 9 to 80 keV. Simulation was performed including the effect of both waviness and bending to fit the experimental data as shown in figure 8. Waviness is a parameter which models the random tilt of the glass surface. The waviness was determined to be 0.15 mrad and the unintentional bend of "straight" fibers to be R = 125 m. In addition to the unintentional bending, the design of the optic requires bending at decreasing radii from the center (R = ∞) to the outer edge (R = 5.57 m) of the optic. The effect of approximating with circular bending is subtracted from the simulation in figure 7.

2.2 Uniformity

Uniformity scans were collected for 15 seconds with a movable 2.1 mm pinhole at the output of the optic. Uniformity scans convey information of any defects in the fibers. Uniformity scans with an energy window of 2 keV were centered at various energies are shown in figure 7. At Mo Kα, the rms uniformity of the center 4.5 mm of the field is 3 %.

2.3 Divergence

The output beam is not completely parallel. There is local divergence, which emerges from each channel due to the critical angle, and global divergence, which is the fiber misalignment due to deviation of the individual channel axis direction from the optical axis.

The experimental set-up for measuring the divergence is shown in figure 10. The silicon crystal is rotated to scan the (400) Bragg reflection for Cu Kβ radiation. Since the mosaicity and the Darwin width of the silicon diffraction rocking curve are very much smaller than the measured divergence, the contribution of the crystal to the rocking curve can be neglected. Figure 11 shows the rocking curve with a width of about 3.9 mrad FWHM. The divergence is about θ_c at 8.9 keV, which requires good fiber alignment.

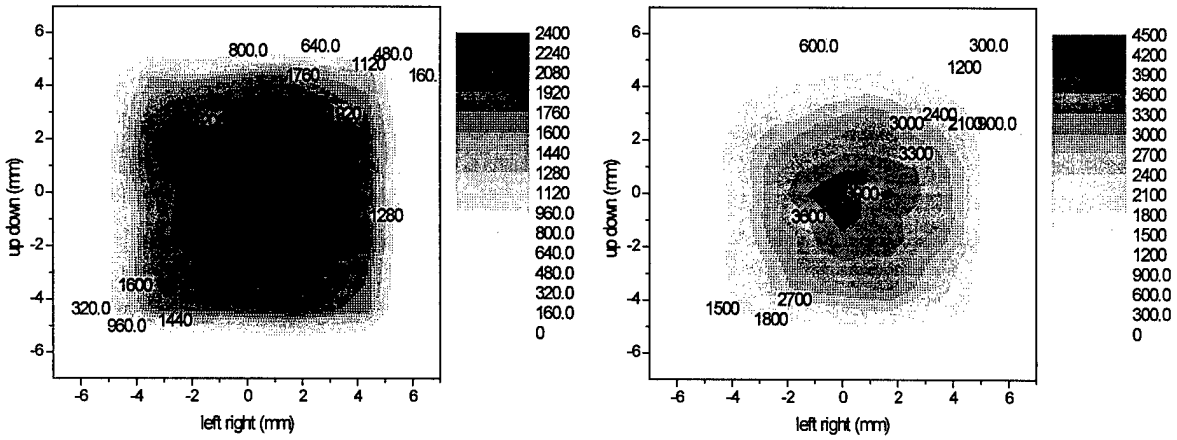

Figure 9. Uniformity scan at molybdenum Kα line 17.5 keV, and 22 keV, respectively.

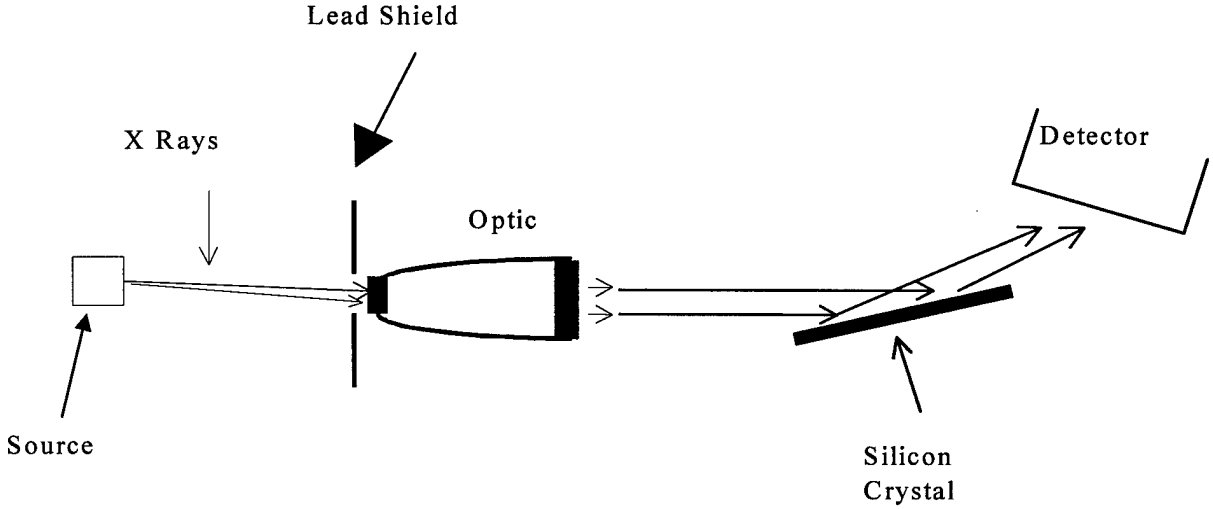

Figure 10. Experimental set-up for exit-angle measurements

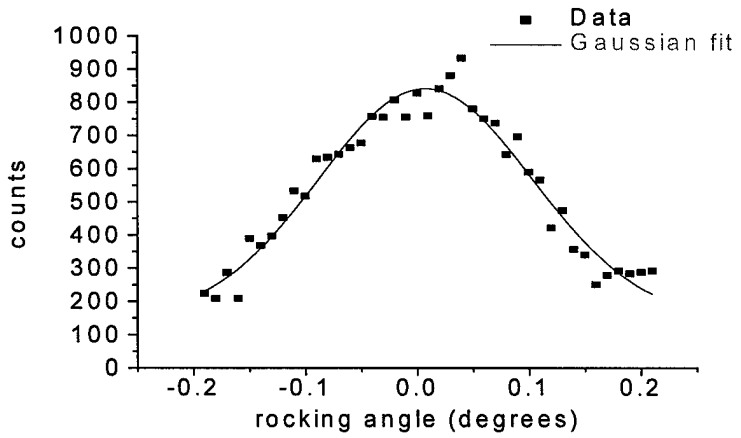

Figure 11. Exit angle divergence data fitted to a Guassian (FWHM is 3.9 ± 0.1 mrad.)

3. MONOCHROMATIC IMAGING

3.1 Intensity

Monoenergetic beams are usually produced with expensive sources such as synchrotrons and free electron lasers. Contrast between carcinoma and breast parenchyma that is usually indistinguishable due to small differences in linear attenuation coefficient; it can be significantly enhanced by the use of monochromatic beams.[4, 5] Here, we used polycapillary optics to obtain adequate intensity from a conventional source. In addition, the parallel beam produced with multi-fiber collimating optics followed by a monochromator crystal renders possible an adequately large air gap to avoid Compton scattered photons at the detector plane.

From section 2.3, the measured Gaussian width, σ = FWHM/(2$\sqrt{}$ln2), for the rocking curve is 2.4 mrad at 8.0 keV. The fraction accepted by a silicon crystal with angular acceptance angle α is given by

$$f(\alpha)=\frac{1}{\sigma\sqrt{\pi}}\int_{-\alpha/2}^{\alpha/2} e^{-\left(\frac{\theta}{\sigma}\right)^2} d\theta \qquad (1)$$

For α = 0.02 mrad, the fraction accepted from the copper $K\alpha_1$ line is 0.5%. If the divergence of the incoming beam is greater than the Bragg angle spread induced by the emission line width, as in this case here, then the percentage of photons reflected by the crystal is obtained by multiplying the angular fraction f(α) by the efficiency of reflection, which is almost unity in this case. The experimental value was determined with a 7.0 - 9.0 keV energy window, and an Amptec detector behind the optic. The silicon crystal reflected 0.3 ± 0.1 % of the intensity, which is in fair agreement with the calculated value.

3.2 Phantom Design

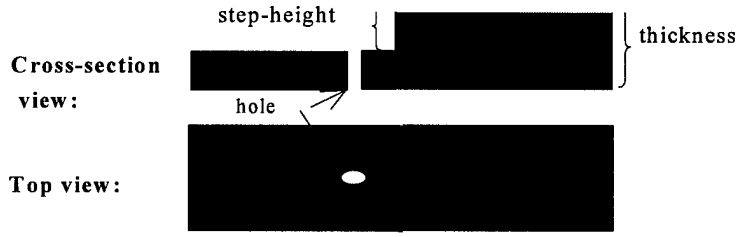

Figure 12. Phantom design using polypropylene plastic

For mammography, 20 keV energy is required. However, the most intense source available in our laboratory is a copper rotating anode at 8 keV. The phantoms designed for this energy are shown in figure 12. They have different step heights to produce the contrast. Images were obtained without optic (conventional, polychromatic), with optic (parallel beam, polychromatic) and with optic and crystal combination (monochromatic) and are shown in figure 13. The phantoms are made from polypropylene plastic, which has a density of 0.90 g/cm^{3}and a linear attenuation coefficient of 3.98 cm^2/g.

3.3 Contrast

Subject contrast is defined as C =ln(I_o/I_p) where I_o is the intensity through the object, which in mammography is the carcinoma, or in this case the thinner side of the phantom. Ip is the intensity through the adjoining area, which is the adjoining soft tissue of the patient, or in this case the thicker side of the phantom

Phantom images were taken with no optic and at 43 cm from the optic for the with optic polychromatic case. This distance is equal to the sum of the distances between the optic and the crystal, 18 cm, and the crystal to the detector, 25 cm, in the monochromatic case. Table 2 shows the contrast of the different step heights. The measurements verify that there is no contrast difference between the no optic and the parallel beam polychromatic case. None is expected as they use the same broad spectrum of radiation, 7-19 keV. The theoretical values averaged over that spectrum agree well with the data. The monochromatic contrast is much higher, by about a factor of 5, and also agrees well with the calculation. Calculated subject contrast enhancement of a 60-mm PMMA phantom at 20 keV, compared to 16-30 keV, is a factor of 2. Another factor of ~ 2 will arise due to removal of scatter. Thus the mammographic contrast enhancement of about a factor of 4 is expected with a simultaneous decrease in dose.[6]

Step height (mm)	Polychromatic			Monochromatic		Ratio	
	Data without optic	Data with optic	Theory	Data	Theory	Data	Theory
1.5	0.2 ± 0.1	0.2 ± 0.1	0.2	0.6 ± 0.2	0.6	3.0 ± 2.0	3.0
2.0	0.2 ± 0.1	0.4 ± 0.2	0.2	0.7 ± 0.2	0.7	3.5 ± 2.0	3.5
4.0	0.4 ± 0.1	0.5 ± 0.2	0.3	2.2 ± 0.3	1.4	5.5 ± 1.1	4.7
7.5	0.7 ± 0.1	0.8 ± 0.2	0.7	4.2 ± 0.3	2.6	6.0 ± 1.5	3.7
15.5	1.2 ± 0.1	1.1 ± 0.3	1.2	5.3 ± 0.4	5.2	4.4 ± 0.7	4.4

Table 2. Contrast variations resulting from polychromatic no optic and with optic cases, and monochromatic case with optic and crystal.

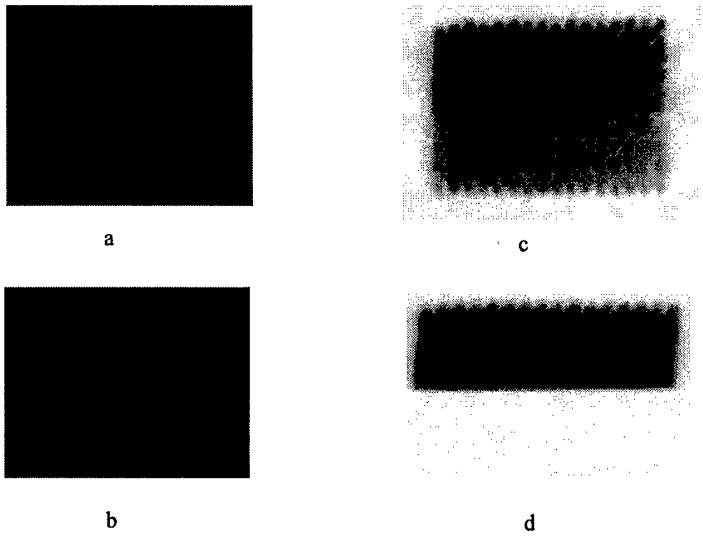

Figure 13. Contrast images using polypropylene plastic. First column (a, b) is polychromatic and second column (c, d) is monochromatic. Hardly no step is visible in the polychromatic images. First row (a, c) has step-height of 1.5 mm and second row (b, d) has 15.5 mm.

4. POST-PATIENT OPTICS: LINEAR MAGNIFYING TAPERS

Monolithic optics are designed as a single piece of glass; the metal grids to hold the fibers are not required. Linearly tapered optics can magnify the image without an increase in geometric blur, as shown in figure 14. The optics also absorb high angle scattered radiation. These optics have been shown to increase system MTF and contrast.[7] However, optics defects have resulted in optics with poor transmission and a low yield of optics with good transmission. A careful characterization and defect study was performed to analyze the problem.

4.1 Transmission and Characterization

The transmission as a function of energy was measured with a molybdenum source and a high purity germanium detector. The transmission of taper I and II are shown in figure 15. The optic parameters are shown in table 3. Source scans at various source to optic distances, similar to figure 3, are shown for taper II in figure 16. The minimum scan width occurs at 31 cm. At distances closer and longer than 31 cm, the width of the source scan widens. All these source scans demonstrate the ability of tapered optics to efficiently reject off-axis radiation, a property required of an anti-scatter grid. Source scans were also carried out at different energies at the 31 cm

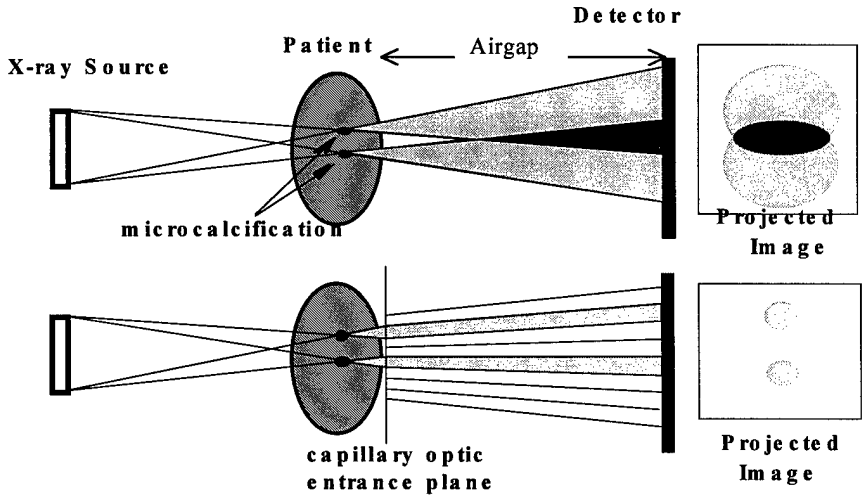

Figure 14 Tapered optics magnify without increasing the geometric blur, as usually occurs with an airgap in the projected image from conventional mammography.

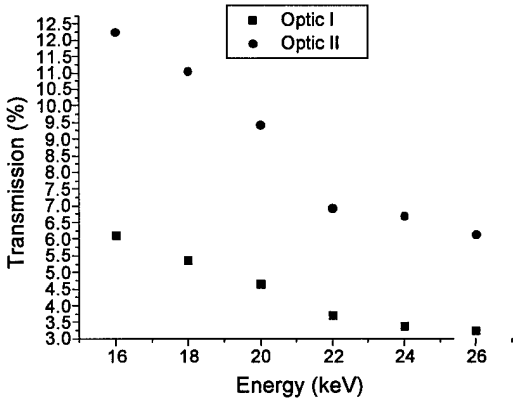

Figure 15. Transmission as a function of energy for taper I and II.

distance shown in figure 17. The higher the energy the narrower the source scan width. This is the result of the smaller critical angle for total reflection at higher energies.

Transmission uniformities of the optic were measured with a pinhole scanned across the output beam. Figure 18 shows the contour maps at different energies. The central core of the optic transmits well, up to high energies, indicating that their profile is very straight. The outer channels are slightly warped, which has more impact at high energies, where the critical angle is smaller.

4.2 Prototype I: Defect Analysis

The poor transmission for taper I was additionally analyzed by sectioning the optic into pieces, as shown in figure 19. The original optic was 32 cm

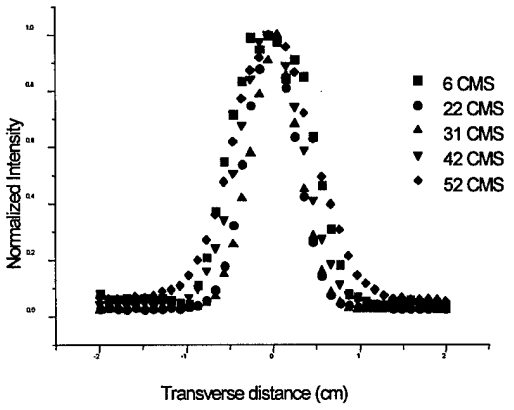

Figure 16. Source scans of tapered optic at different source optic distances. The focal length is 31 cm.

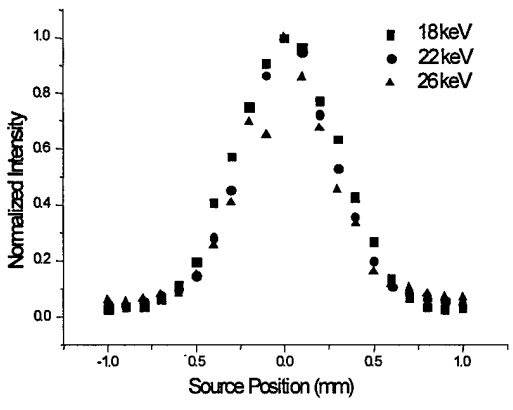

Figure 17. Source scans at different energies.

Parameters	Prototype Taper I	Prototype Taper II
Profile	Linear	Linear
Input diameter	2 mm	1.9 mm
Output diameter	4 mm	3.82 mm
Input channel diameter	5 μm	4.9 μm
Output channel diameter	10 μm	9.8 μm
Optic length	320 mm	350 mm
Transmission efficiency @ Mo K lines	5 – 7 %.	9 – 12 %.

Table 3. Tapered optics parameters.

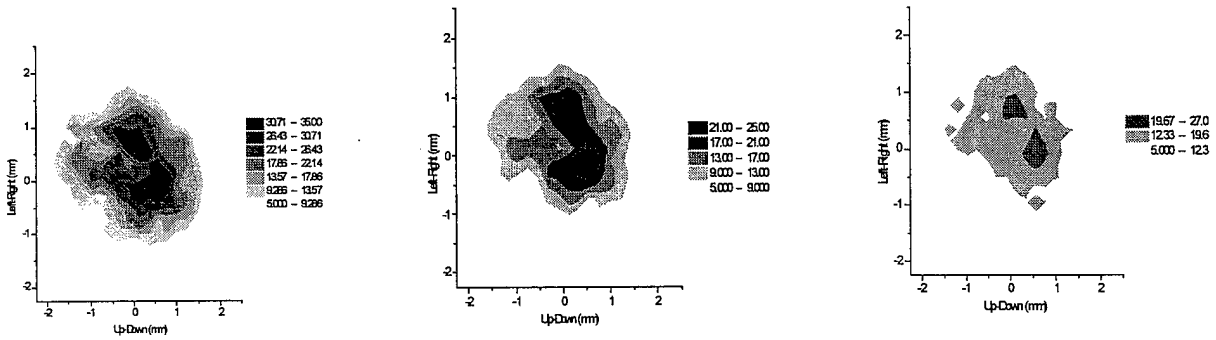

Figure 18. Transmission uniformity at 14 keV, 18 keV, and 22 keV, respectively.

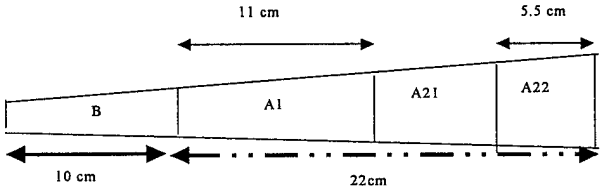

Figure 19. The taper was sectioned to investigate the defect structure.

long. The optic was sectioned with a razor blade. The transmission of the original optic and the 22 cm and 10 cm pieces are shown in figure 20.

The inset in figure 20 shows the output images of the two sections, with a defect blocking parts of section A. This section was further divided into two 11 cm pieces, named A1 and A2. The transmissions of the three pieces are shown in figure

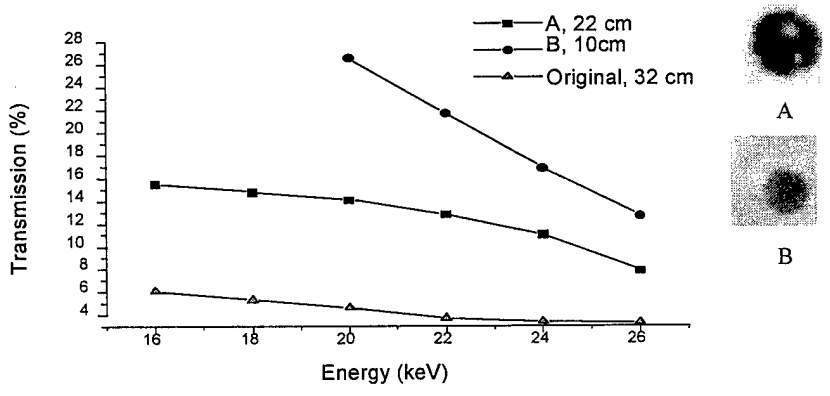

Figure 20. Transmission as a function of energy for original taper I and its component pieces. Insets are x-ray images of the outputs, taken with T57 polaroid film, showing a defect in piece A.

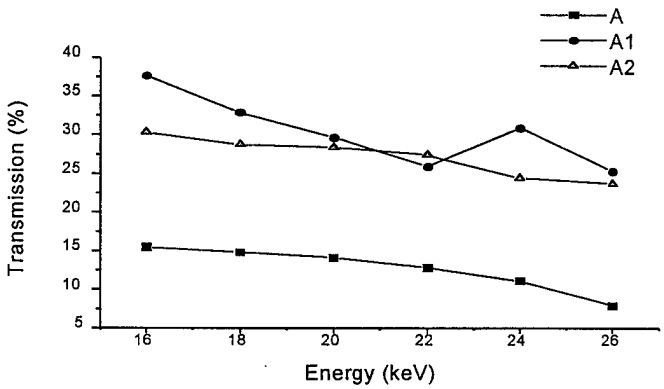

Figure 21. Transmission as a function of energy for the 22 cm optic section A and its components A1 and A2, each 11 cm long

21. The dip in transmission indicates that there is glass blockage in A1. However, the image shows glass inclusions in A2 as well. A2 was further sectioned into A21 and A22 of equal length (5.5 cm). The transmission of the A2 and its respective pieces are shown in figure 22. The inclusion in A2 has been localized to A21. The output of A22 is uniform out to the hexagonal edges. The transmission of A21 has a minima around 20 keV, not seen in A22. The minima is a result of competition between the normal decrease in transmission with energy, which is a result of the decrease in critical angle with energy, and an increase with energy of penetration through glass inclusions blocking the channels. Optical microscope images confirm the presence of glass blockages. This defect is clearly seen in figure 23, which demonstrates the blockages in channels and fused regions.

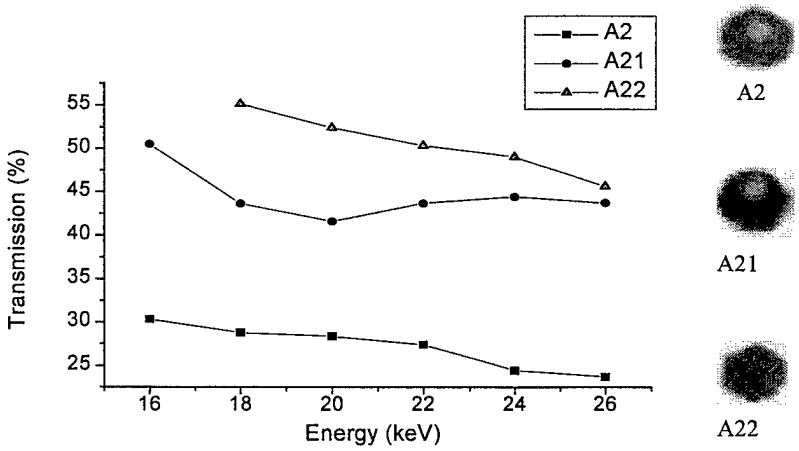

Figure 22. Transmission as a function of energy for A2 and its component pieces, A21 and A22.

Figure 23. Optical microscope images of the defected piece A21. Note the glass blockages and fused regions.

4.3 Manufacturing Improvements

The defects detected in section 4.1 and 4.2 were outer channel warping and glass inclusions. These resulted in poor optic transmission. Improvements in manufacturing technique designed to mitigate these problems, performed by the supplier, has resulted in optics with much higher transmission, around 50% at 20 keV, shown in figure 24. The inset is the output of the tapered optic taken with the image plate. It is uniform out to the hexagonal edges.

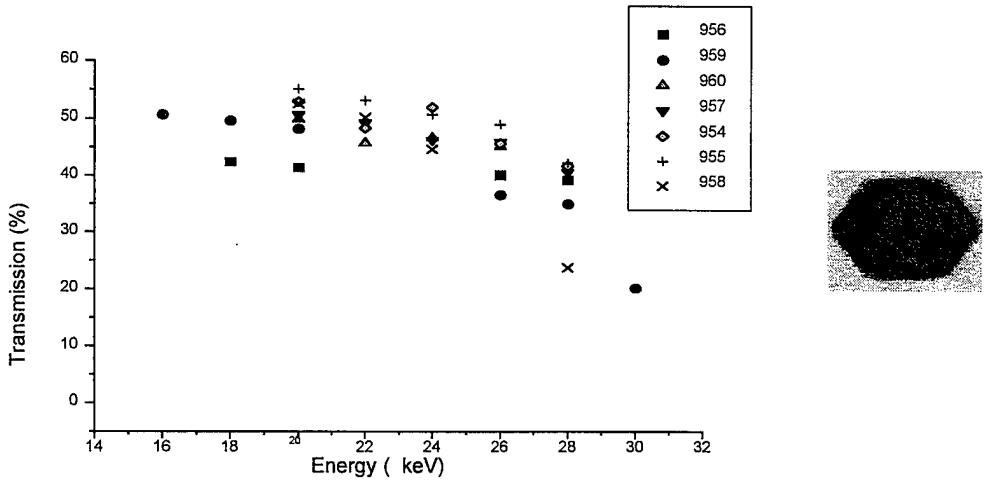

Figure 24. Transmission as function of energy for newly manufactured tapers. Inset is the image-plate output of the optic. Note the uniformity out to the hexagonal edges.

5. CONCLUSIONS

Both pre-and post-patient polycapillary optics have been characterized to show their individual potential for mammographic imaging. Using collimating optics to produce a monochromatic beam, a contrast enhancement of 5 was measured at 8 keV compared to the polychromatic conventional case. At 20 keV, a contrast ratio of 4 is expected.

The advantage of post-patient optics is high scatter rejection and blur-free magnification. These optics can now be manufactured with a repeatable transmission of 50%.

ACKNOWLEDGEMENTS

The authors would like to express their gratitude to their colleagues at the Center for X-ray Optics, and to X-ray Optical Systems for providing the optics. This research is funded by the U.S. Army Breast Cancer Research Program and the National Institutes of Health.

REFERENCES

[1] M. A. Kumakhov and F. F. Komarov, " Multiple Reflections from Surface X-ray Optics, " *Phys. Rev.*, **191**, pp. 289-350, 1990.

[2] Qi-Fan Xiao, Igor Yu Ponamarev, Alexandre I Kolomitsev and John C. Kimball. " Numerical Simulations for Capillary-Based X-ray Optics," *X-ray Detector Physics and Applications*, SPIE Vol. **1736**, 1992, pp.227-238

[3] Hui Wang, Lei Wang, W. M. Gibson, C.A. MacDonald, "Simulation Study of Polycapillary X-Ray Optics, " *X-Ray Optics, Instruments, and Missions*, SPIE Vol.**3444**, 1998, pp.643-651.

[4] J. M. Boone and J. A. Seibert, "A Comparison of Mono- and Poly-energetic X-ray beam Performance for Radiographic and Fluoroscopic Imaging." *Med. Phys.* **21**(12), 1853, 1994.
[5] R. J. Jennings, P. W. Quinn, R. M. Gagne and T. R. Fewell, "Evaluation of X-ray Sources for Mammography," *Physics of Medical Imaging*, SPIE Vol. **1896**, 1993, pp. 268-259.
[6] Cari, S. D. Padiyar, C. A. MacDonald, W. M. Gibson, C. D. Alexander, M. K Joy, C. H. Russell, Z. Chen, "Characterization of a Long-focal-length polycapillary Optic for High Energy X-Rays," *Advances in Laboratory-Based X-ray Sources and Optics*, SPIE Vol. **4144**, 2000.
[7] D. G. Kruger, C. C. Abreu, E. G. Hendee, A. Kocharian, W. W. Peppler, and C. A. Mistretta. "Imaging Characteristics of X-ray Capillary Optics in Digital Mammography," *Med. Phys.*, **23**(2), 187-196, February 1996.

Monochromatic Imaging with a Conventional Source Using Polycapillary X-ray Optics

Francisca R. Sugiro, C. A. MacDonald*
Center for X-ray Optics, University at Albany, State University of New York,
Albany, New York 12222

ABSTRACT

Monochromatic parallel beam imaging produces high subject contrast, high resolution, and low patient dose. Polycapillary collimating optics can be used to create a beam of sufficient intensity for monochromatization from a conventional source. Monochromatization is achieved by diffraction from a single crystal. Contrast, resolution, and intensity measurements were performed with both high and low angular acceptance crystals. Testing was first done at 8 keV with an intense copper rotating anode, then preliminary 17.5 keV measurements were made with a low power molybdenum source. At 8 keV, contrast enhancement was a factor of 5 relative to the polychromatic case, in good agreement with theoretical values. At 17.5 keV, monochromatic subject contrast is a factor of 2 times greater than the conventional polychromatic contrast. An additional factor of two increase in contrast is expected from the removal of scatter obtained from using the air gap which is allowable from the parallel beam. The measured angular resolution after the crystal was 0.6 mrad for a silicon crystal. The use of polycapillary collimating optics allowed monochromatic imaging measurements using a conventional rotating anode source and computed radiography plate in 300 mAs.

Keywords: polycapillary optics, collimation, monochromatization, contrast, resolution

1. INTRODUCTION

Conventional imaging has been hampered by the somewhat wide spectrum of radiation emitted by x-ray tubes. Soft x-rays only increase patient dosage. On the other end of the spectrum, high energies produce less subject contrast and give rise to scattered radiation, which reduces visibility of structures within the tissues. Monochromatic beams give maximum intensity at the optimum energy and increase the difference between linear attenuation coefficients compared to the usual average values over a wide energy range.[1,2]

Monochromatic imaging has previously been available only for high intensity sources such as synchrotrons and free electron lasers. High diffracted beam intensity can be achieved with collimating multi-fiber polycapillary optics in combination with a conventional laboratory sources. These optics consist of hundreds fibers which are laced through a metal grid. The fibers at the entrance point at the x-ray source and are parallel at the other end. These fibers in turn consist of hundreds of hollow channels, along which x rays can travel by total external reflection. The critical angle for total reflection is

$$\theta_c\ (mrad) = \frac{E_p}{E(keV)} \qquad (1)$$

where Ep is the plasma energy for borosilicate glass, ~31 eV, and E is the x-ray energy.

In order to refine future modeling for imaging, computer simulations based on Monte Carlo simulations of simple geometrical optics were compared to optics measurements. The characterization for these prototype optics agree quite well with the simulations. Table 1 summarizes both the manufacturing parameters and the experimental results for the collimating optic.[3,4]

The monochromator crystal deflects the beam after it passes through the collimating optic. The Bragg angle deflection is

$$\theta_B = \sin^{-1}\left(\frac{\lambda}{2d}\right) \qquad (2)$$

* email: c.macdonald@albany.edu

where d is the crystal lattice plane.

A collimating optic/crystal combination is essential to create an x-ray beam intensity sufficient for rapid imaging. Either the optic or crystal when using alone is problematic. The essential difficulty in using a collimating optic alone (aside form the lack of monochromaticity) lies on the output divergence of each polycapillary channel. The output divergence is approximately equal to $1.5*\theta_c$ of the optic. Therefore, a collimating optic does not give a completely parallel beam. For a 50-mm thick sample, the geometrical blur at 20 keV would be 100 μm or a resolution of 5 line-pairs/mm. This is insufficient resolution for imaging; therefore, a diffracting crystal must be incorporated with the optic to reduce angular divergence. The major problem in using a crystal alone to monochromatize a conventional source is obtaining sufficient beam intensity. The reflection efficiency of a diffracting crystal depends on its angular bandwidth. Large bandwidth such as obtained with graphite yields good intensity, but insufficient resolution. On the other hand, small bandwidth as obtained with silicon gives high resolution but low intensity.

Collimating Optic	
Length	127 mm
Field shape	square
Input size	8.1 by 8.1mm
Output size	10 by 10 mm
Focal distance	250 mm
Acceptance angle	1.8 °
Fiber diameter (flat to flat)	510 μm
Channel diameter	10 μm
Depth of field	10 mm
Transmission (6.5 –19.5 keV)	39 %
Output angular divergence at 8.9 keV	4.0 mrad

Table 1. Optic parameters.

In addition to monochromatiztion, the optic/crystal combination produces a parallel beam. The extremely parallel beam from the crystal allows the use of an air gap before the detector, reducing the scattered radiation and therefore enhancing the contrast. Additional advantages of using parallel beams are elimination of image distortion from the different magnification of objects on the entry and exit side of the patient, elimination of variations in resolution from the different apparent source sizes, and relaxation of geometrical restraints that have affected system design.

2. EXPERIMENTAL RESULTS AND DISCUSSIONS

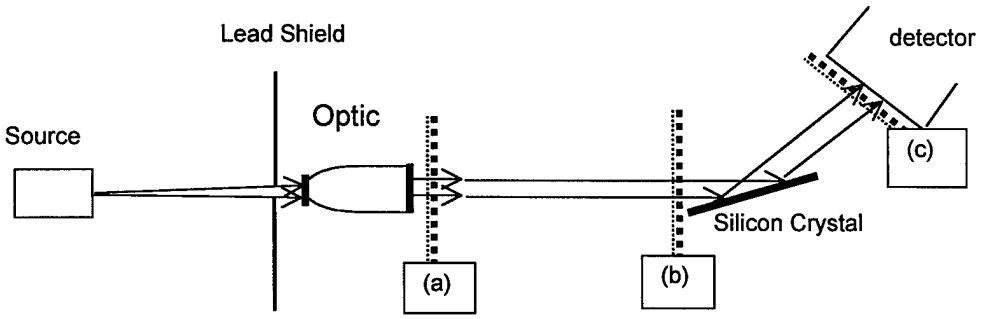

Figure 1. Experimental Set-up

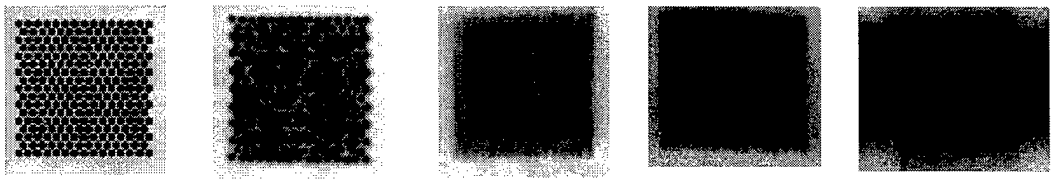

(a) (b) (c1) (c2) (c3)

Figure 2. X-ray images of the filed at the locations marked (a) –(c) in figure 1. The fiber structure of the optic is clearly visible in (a). Location of (b) is 17 cm after the optic. The divergence has blurred the fiber structure. Post crystal images are measured using a Fuji image plate for silicon (400) (c1), for mica (0010) (c2) and for graphite (002) (c3).

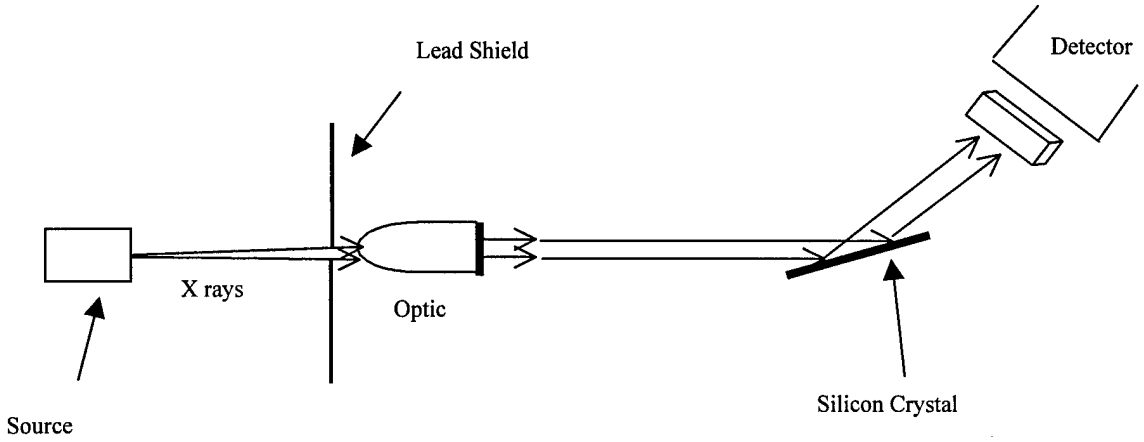

Figure 3. Monochromatic contrast measurement set-up.

The experimental arrangement for monochromatic imaging with the optic is shown in figure 1. The copper rotating anode was used at 20 kVp and 10 mA. The optic and crystal are on linear and rotation stages and actuators for accurate alignment to the x-ray beam. The beam produced by the optic before and after the crystal is shown in figure 2. The divergence from the optic can be used to blur the fiber structure.

2.1 Contrast at 8 keV

Contrast was taken as

$$C \equiv \ln\left(\frac{I_1}{I_2}\right) \qquad (3)$$

where I_1 is the intensity through the area of interest and I_2 for an adjacent area. The intensity through a solid medium of thickness t is given by

$$\frac{I_t}{I_o} = e^{-\left(\frac{\mu}{\rho}\right)\rho t} \qquad (4)$$

where μ/ρ is the mass absorption coefficient, t is the distance traveled, and I_o and I_t are the intensities of the incident and transmitted beam respectively.

Polypropylene step phantoms of different heights were tested in the polychromatic and monochromatic cases. For the latter case, the phantom was placed after the crystal and before the detector as shown in figure 3. In the polychromatic case images were taken with the phantom placed before the optic. The images are taken with a 50-micron resolution imaging plate with an exposure of approximately 300 mAs (at 8 keV). The construction of these phantoms with different step height is shown in figure 4.

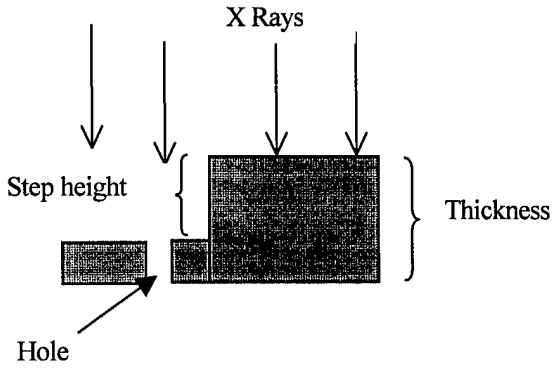

Figure 4. Shape of the polypropylene step phantom used for figure 5 and table 2.

The contrast arising from the two thicknesses are compared in both the conventional and the monochromatic cases in table 2. The images for five different step heights are shown in figure 5. In the polychromatic case, the theoretical intensities are averaged from 7 keV to 19 keV. The tube voltage was 20 kVp. The data from all three crystals agree with each other and the theoretical calculation. The contrast enhancement is greater than 5 for monochromatic imaging at 8 keV.

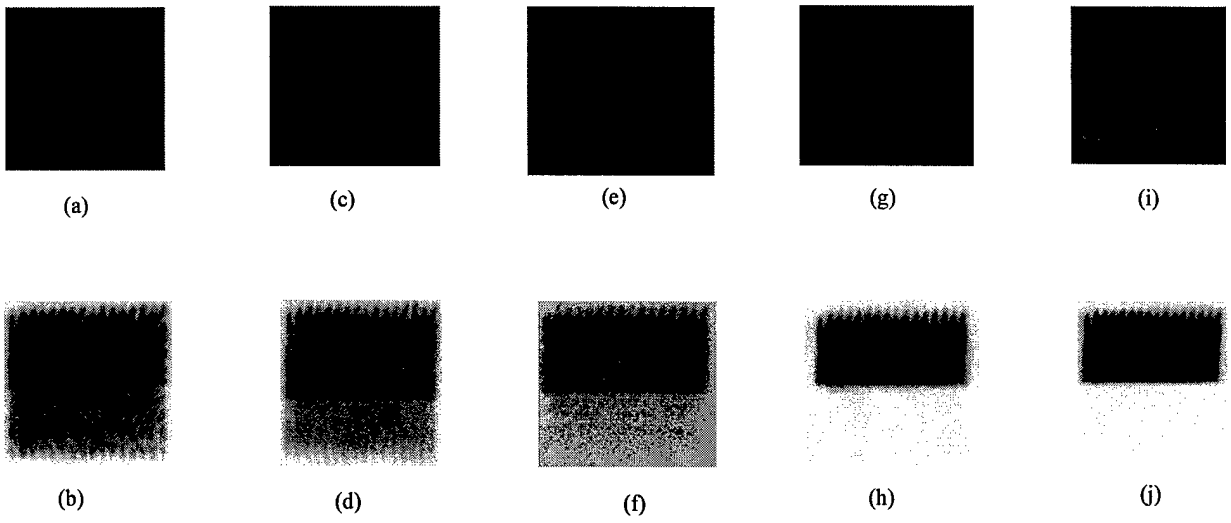

Figure 5. Image plate data from five different polypropylene step phantoms. The top row is measured without optic (conventional), the bottom row is measured in the monochromatic case. Column (a-b) is the phantom with a step height of 1.5 mm, column (c-d) with 2.0 mm, column (e-f) with 6.6 mm, column (g-f) with 10.6 mm, and column (i- j) with 15.5 mm. Notice contrast is already visible in the monochromatic case for a even for the lowest step height.

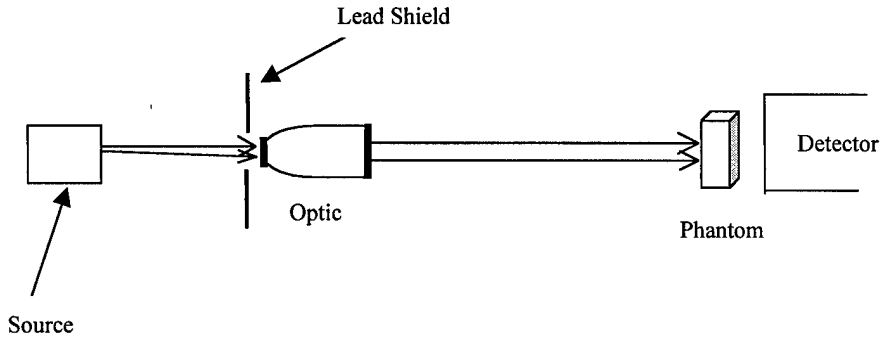

Figure 6. Experimental set-up for parallel beam imaging.

In addition to the step phantoms, monochromatic images were also measured for a phantom consisting of two compositions of plastic, polypropylene (PP) and polyvinyl chloride (PVC) with the approximately the same thickness (0.5 mm). The density of the plastic was not measured but was taken as 0.9 g/cm3 and 1.4 g/cm3, respectively. The absorption constants were taken from NIST[5] as 3.30 for PP and 87.86 for PVC. Table 3 summarizes the experimental and the theoretical values for both the polychromatic and monochromatic cases.

To verify that the contrast enhancement was due to the monochromatization, and not due to the parallel beam, step phantoms were measured with and without optic with the set-up shown in figure 6. Contrast with and without the optic is shown in table 4, and, as expected, are in agreement. The agreement in table 2 between the different crystals further indicates that the contrast is also unaffected by the crystal bandwidths.

Step-height (mm):	Polychromatic Contrast:	
	Data: (without optic)	Theory:
1.5	0.2 ± 0.1	0.2
2.0	0.2 ± 0.1	0.2
6.6	0.4 ± 0.1	0.4
10.6	0.8 ± 0.1	0.8
15.5	1.2 ± 0.1	1.2

Step-height (mm):	Monochromatic Contrast:			
	Data:			Theory:
	Silicon:	Mica:	Graphite:	
1.5	0.6 ± 0.4	0.7 ± 0.1	0.7 ± 0.3	0.6
2.0	0.7 ± 0.3	0.9 ± 0.2	1.0 ± 0.2	0.7
6.6	2.2 ± 0.5	1.8 ± 0.3	2.1 ± 0.2	2.2
10.6	4.3 ± 0.5	3.8 ± 0.2	4.2 ± 0.3	3.8
15.5	5.3 ± 0.4	5.2 ± 0.2	5.1 ± 0.5	5.2

Step-height (mm):	Data Contrast Ratio:			Theory Contrast Ratio:
	Silicon:	Mica:	Graphite:	
1.5	3.0 ± 2.6	3.3 ± 1.3	3.6 ± 2.6	3.0
2.0	4.1 ± 2.5	5.4 ± 2.2	5.8 ± 2.6	3.5
6.6	5.4 ± 2.5	4.6 ± 1.8	5.4 ± 1.9	5.7
10.6	5.3 ± 1.1	4.6 ± 0.7	5.2 ± 0.8	4.8
15.5	4.4 ± 0.6	4.3 ± 0.5	4.2 ± 0.7	4.3

Table 2. Comparison for step phantoms of contrast with silicon, mica, and graphite crystals to the polychromatic contrast for conventional imaging.

Cases:		Contrast:		Contrast Ratio:	
		Data	Theory	Data	Theory
Polychromatic:		0.5 ± 0.1	0.5		
Monochromatic:	silicon	3.0 ± 0.3	2.9	6.4 ± 2.2	6.0
	mica	3.0 ± 0.4		6.4 ± 2.5	
	graphite	2.6 ± 0.2		5.5 ± 1.9	

Table 3. Contrast of different compositions in both the poly- and monochromatic cases.

Step height (mm):	Without optic	With optic:
1.5	0.2 ± 0.1	0.1 ± 0.2
2.0	0.2 ± 0.1	0.4± 0.3
6.6	0.4 ± 0.1	0.5 ± 0.1
10.6	0.8 ± 0.1	0.8 ± 0.1
15.5	1.2 ± 0.1	1.3 ± 0.2

Table 4. Verification that the contrast is not changed by the optic alone.

2.2 Preliminary Contrast Measurements at 17.5 keV

An ultra-bright molybdenum Oxford source with tube voltage of 25kVp and low power (10-20 W) was used to measure 45-mm Lucite phantoms with different hole depths. Each depth was compared without optic and with a combination of optic and crystal at molybdenum Kα line. The theoretical contrast was averaged over 8 to 25 keV. A contrast enhancement of more than a factor of 2 is found experimentally, which agrees with the theoretical calculations.

Table 5 summarizes the results. Further measurements will be performed with optics designed to give optical performance with this source, and also with large area illumination, to include the effects of scatter. Because the useable phantoms are quite thin at 8 keV, and the beam at 17.5 keV was very narrow, there was essentially no scatter in any of these measurements. An additional contrast enhancement is expected from using either a parallel beam air gap or a straight post phantom polycapillary optic to remove the scatter.[6,7]

Depth (mm)	Polychromatic Contrast		Monochromatic Contrast	
	Data	Theory	Data	Theory
35	1.3 ± 0.1	1.3	2.4 ± 0.3	2.9
30	1.2 ± 0.1	1.0	2.1 ± 0.3	2.5
20	0.8 ± 0.1	0.6	1.4 ± 0.4	1.7
15	0.4 ± 0.1	0.5	0.7 ± 0.4	0.8

Depth (mm)	Contrast Enhancement Ratio:	
	Data	Theory
35	1.8 ± 0.6	2.2
30	1.8 ± 0.4	2.5
20	2.2 ± 0.9	2.8
15	1.5 ± 0.9	1.6

Table 5. Contrast at 17.5 keV with 45-mm Lucite phantom.

2.3 Resolution

The output divergence of the optic affects the resolution and is an important parameter especially for low energy and high resolution modalities. The exit divergence from capillary optics is measured by rotating a high quality crystal (usually silicon) in the beam and by measuring the angular width of a Bragg peak. For the narrowest bandwidth crystal, silicon, the entire rocking curve width is due to the optic divergence. For mica, the width is a combination of the divergence and the crystal width. For graphite, the crystal dominates. The rocking curves for the Kα copper line measured with each of the three crystals are shown in figure 7.

A knife-edge made of tantalum was placed after the monochromatic parallel beam. An image plate was placed 300 mm from the knife-edge to overcome the 50-μm resolution. Tantalum was chosen so to reduce the x-ray fluorescence background. The intensity profile of the direct beam to the knife-edge side can be measured. The derivative of the intensity profile can be calculated, which consists of the resolved doublet of $K\alpha_1$ and $K\alpha_2$. The gaussian width of the $K\alpha_1$ line is given in table 6 for silicon, mica and graphite crystals. The intensity profile measured with silicon, mica, and graphite crystals are shown in figure 8.

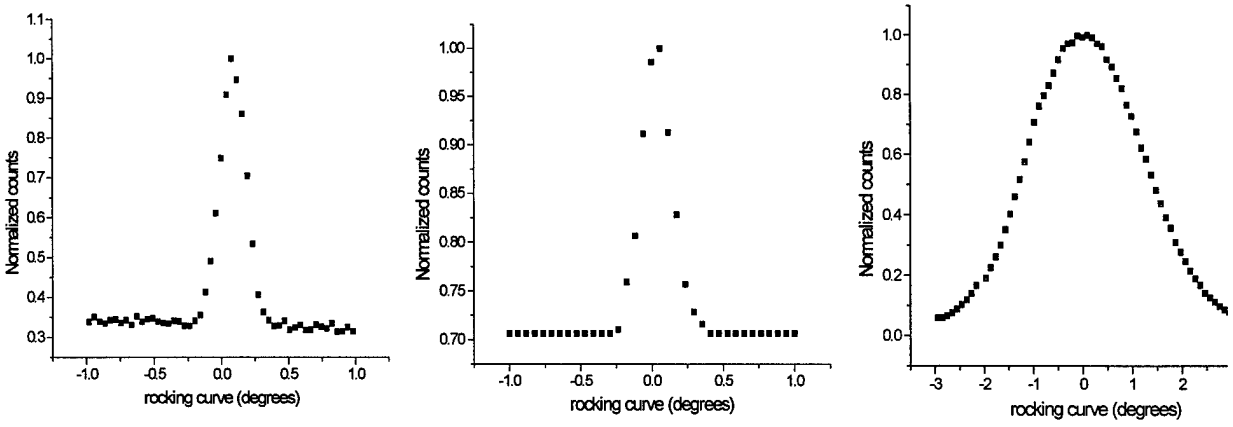

Figure 7. Rocking curves of three crystals: silicon (a) with FWHM 4.0 mrad, mica (b) with FWHM 4.4 mrad, and graphite (c) with FWHM 42.5 mrad. Note the change in scale for graphite rocking curve.

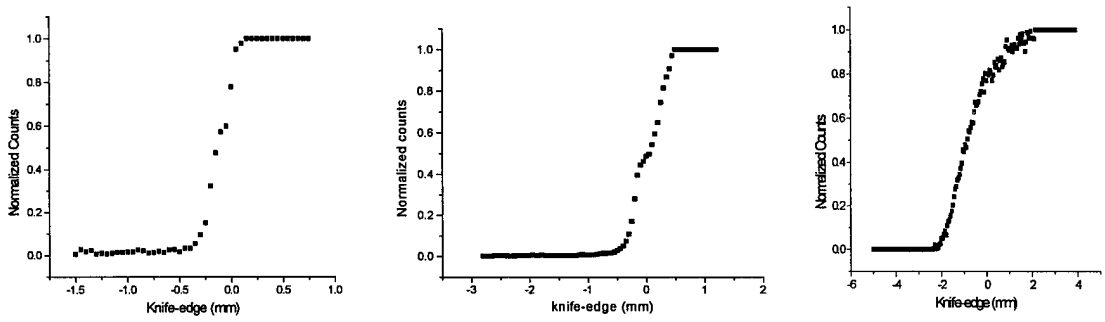

(a) (b) (c)

Figure 8. Resolution profiles obtained with silicon (a), mica (b) and graphite (c) crystals incident angles.

For a perfect crystal and parallel monochromatic input beam, the knife-edge image would be ideally sharp (with a perfect detector). For a crystal with a large bandwidth, such as graphite, the angular width is determined by the optic divergence, since the crystal can accommodate the full range of angles output from the optic. For a crystal with a bandwidth narrower than the optic divergence, a monochromatic beam would give a width equal to the crystal bandwidth. The 3-eV energy width of the $K\alpha_1$ emission line produces an additional angular spread of

$$\sigma_E \equiv \tan\theta_0 \frac{\sigma_{K\alpha_2}}{E_{K\alpha_2}} \approx 0.4\,\text{mrad} \tag{5}$$

Combining the effects of the crystal, optic divergence, and energy spread, the angular distribution of intensity off the crystal should be given by a Gaussian distribution,

$$I(\Delta\theta) = \int\int I(\varphi)I(E(\beta))p(\beta)\delta(\Delta\theta - \varphi + 2\beta)d\varphi dE = \frac{\alpha}{2\sqrt{\pi}\sigma_{optic}\sqrt{\alpha^2+\sigma_E^2}} e^{-\frac{\Delta\theta^2}{\sigma^2}}, \tag{6}$$

where $\Delta\theta$ is the deviation of the output angle from the normal Bragg angle, $I(\phi)$ is the angular distribution from the optic, assumed to be a Gaussian of width σ_{optic}, $I(E)$ is the spectral distribution of the $K\alpha_1$ line, also assumed Gaussian of width σ_E, $\beta(E)$ is the relationship between angles and energies given by Bragg's law, equation (2), $p(\beta)$ is the probability distribution of the planes at angle β from the surface of the crystal, which has a width α given by the crystal bandwidth, the delta function insures that the incidence angle equals the reflection angle, and

$$\sigma = \sqrt{\frac{4\sigma_E^2\cdot\alpha^2 + \sigma_E^2\cdot\sigma optic^2 + \sigma optic^2\cdot\alpha^2}{\alpha^2 + \sigma optic^2 + \sigma_E^2}}. \tag{7}$$

This is additionally broadened by the detector resolution, which is 50 μm at 300 mm or 0.2 mrad. The experimental angular resolutions, which are taken as the widths of the knife-edge profiles, are shown in table 6. The values agree fairly well with the calculated resolutions, for which the detector broadening in the knife edge measurement has been added in quadrature. The theoretical angular resolution from the optic/crystal system would give a spatial resolution for an object on the front side of a 50-mm thick patient of 23 lp/mm with an ideal detector and the silicon crystal. The resolutions for all three crystals are shown in table 6.

Crystals:	Manufacturer's specification for α (mrad):	Measured rocking curve width (mrad):	Angular width of knife-edge image (mrad):	σ, Theory (mrad), with detector with 50 μm pixels	σ, Theory (mrad), with an ideal detector	Resultant resolution for 50-mm thick patient for an ideal detector (lp/mm)
Silicon	0.02	4.0 ± 0.1	0.54 ± 0.02	0.47	0.43	23
Mica	0.4	4.4 ± 0.2	0.78 ± 0.04	0.52	0.48	20
Graphite	35 – 87	42.5 ± 1.1	6.5 ± 0.5	4.5	4.5	2

Table 6. Rocking curves and resolution measurements using three different crystals. The rocking curve widths are due to the combined effects of the angular bandwidth of the crystal and the 4-mrad output divergence of the optic. The angular resolution calculations are given by equation (7). The energy width for graphite is taken to include the whole Kα doublet.

The efficiency η of a crystal is calculated to be

$$\eta = \int I(\Delta\theta)d\Delta\theta = \frac{\alpha}{\sqrt{\sigma optic^2 + \alpha^2 + \sigma_E^2}} \qquad (8)$$

The intensity reflected by the crystal is η multiplied by the reflectivity, R, of the crystal itself. For silicon, η is 0.005, R is approximately unity, and the measured efficiency is 0.003 ± 0.001. The 8 keV images were given an exposure of 300 mAs.

3. CONCLUSION

Polycapillary collimating optics in combination with conventional laboratory sources produce high enough intensity for monochromatic imaging. Angular bandwidth crystals of 0.02 mrad (silicon), 0.5 mrad (mica), and 42.5 mrad (graphite) have been tested at the copper Kα, 8 keV. Contrast of different step height phantoms was enhanced by a factor of 5 at 8 keV relative to the conventional polychromatic case. Contrast enhancement for a phantom of varying composition was a factor of 6. These all were in good agreement with the theory. The measured angular resolution with a silicon crystal is 0.5 mrad at 8 keV. For a 50-mm thick patient, this angle corresponds to 20 lp/mm. At the molybdenum Kα line, 17.5 keV, a contrast enhancement of 2 was measured with a 45-mm thick Lucite phantom, in good agreement with theory.

ACKNOWLEDGEMENTS

The authors would like to express their gratitude to Dr. Walter Gibson. This research is funded by DOD Breast Cancer Research grant, DAMD179919316 and NIH grants CA77477-03 and CA58521-05.

REFERENCES

[1] J. M. Boone and J. A. Seibert, "A Comparison of Mono- and Poly-energetic X-ray beam Performance for Radiographic and Fluoroscopic Imaging." *Med. Phys.* **21**(12), 1853, 1994.

[2] R. J. Jennings, P. W. Quinn, R. M. Gagne and T. R. Fewell, "Evaluation of X-ray Sources for Mammography," *Physics of Medical Imaging*, SPIE Vol. **1896**, 1993, pp. 268-259.

[3] S. D. Padiyar, Hui Wang, M. V. Gubarev, W. M. Gibson and C.A. MacDonald, "Characterization of Multi-fiber Polycapillary X-ray Collimating Optics," EUV, X-ray, and Neutron Optics and Sources, SPIE Proc.3767, 1999

[4] F. R. Sugiro, S. D. Padiyar, and C. A. MacDonald, "Characterization of Pre-and Post-patient X-ray Polycapillary Optics for Mammographic Imaging," in C.A. MacDonald and Ali M. Khounsary, eds., **Advances in Laboratory-Based X-ray Sources and Optics**, SPIE vol. 4144, 2000.

[5] http://physics.nist.gov/PhysRefData/XrayMassCoef/cover.html

[6] D. G. Kruger, C. C. Abreu, E. G. Hendee, A. Kocharian, W. W. Peppler, and C. A. Mistretta. "Imaging Characteristics of X-ray Capillary Optics in Digital Mammography," *Med. Phys.*, **23**(2), 187-196, February 1996.

[7]Cari, C.A. MacDonald and W.M. Gibson, C. D. Alexander and M.K. Joy, C.H. Russell, Z. W. Chen, "Characterization of a Long Focal Length Polycapillary Optic for High Energy X rays," in C.A. MacDonald and Ali M. Khounsary, eds., **Advances in Laboratory-Based X-Ray Sources and Optics**, SPIE vol. 4144, pp.183-192, 2000.